ELSEVIER

International Journal of Refrigeration 24 (2001) 348–366

REVUE INTERNATIONALE DU FROID
INTERNATIONAL JOURNAL OF
refrigeration

www.elsevier.com/locate/ijrefrig

The effect of lubricant concentration, miscibility, and viscosity on R134a pool boiling☆

M.A. Kedzierski *

National Institute of Standards and Technology, Bldg. 226, Rm B114, Gaithersburg, MD 20899, USA

Abstract

This paper presents pool boiling heat transfer data for 12 different R134a/lubricant mixtures and pure R134a on a Turbo-BII^{TM}-HP surface. The mixtures were designed to examine the effects of lubricant mass fraction, viscosity, and miscibility on the heat transfer performance of R134a. The magnitude of the effect of each parameter on the heat transfer was quantified with a regression analysis. The mechanistic cause of each effect was given based on new theoretical interpretation and/or one from the literature. The model illustrates that large improvements over pure R134a heat transfer can be obtained for R134a/lubricant mixtures with small lubricant mass fraction, high lubricant viscosity, and a large critical solution temperature (CST). The ratio of the heat flux of the R134a/lubricant mixture to that of the pure R134a for fixed wall superheat was given as a function of pure R134a heat flux for all 12 mixtures. The lubricant that had the largest CST with R134a exhibited the greatest heat transfer: 100%±20% greater than that of pure R134a. By contrast, the heat transfer of the mixture with the lubricant that had the smallest viscosity and the smallest CST with R134a was 55%±9% less than that of pure R134a. High-speed films of the pure and mixture pool boiling were taken to observe the effect of the lubricant on the nucleate boiling.

Keywords: Refrigerant; R134a; Pool boiling; Heat transfer; Lubricant; Concentration; Miscibility; Viscosity

Effet de la concentration du lubrifiant, de la miscibilité et de la viscosité sur l'ébullition libre de R134a

Résumé

Cette communication présente les données sur le transfert de chaleur lors de l'ébullition libre de 12 mélanges de R134a avec des lubrifiants et pour le R134a pur sur une surface Turbo-BII^{TM}-HP. Les mélanges ont été concus afin d'étudier les effets le la fraction massique, la viscosité et la miscibilité sur la performance de R134a en termes de transfert de chaleur. L'ampleur de l'effet de chaque paramètre sur le transfert de chaleur a été quantifiée l'aide d'une analyse de régression. La cause mécanique de chaque effet est fournie en se fondant sur une nouvelle interprétation théorique et/ou une interprétation fondée sur les données publiées. Le modèle montre que de grandes améliorations peuvent être obtenues pour le transfert de chaleur des mélanges R134a/lubrifiant avec une faible fraction massique, une viscosité du lubrifiant élevée et une température de solution critique (CST) plutôt élevée. La relation flux thermique du mélange R134a/lubrifiant par rapport au

☆ Certain trade names and company products are mentioned in the text or identified in an illustration to adequately specify the experimental procedure and equipment used. In no case does such an identification imply recommendation or endorsement by the National Institute of Standards and Technology, nor does it imply that the products are necessarily the best available for the purpose.

* Tel.: +1-301-975-5282; fax: +1-301-975-4032.
E-mail address: mark.kedzierski@nist.gov

0140-7007/01/$20.00
PII: S0140-7007(00)00030-X

flux thermique de R134a pur pour une surchauffe de la paroi fixe est donnée en fonction du flux thermique de R134a pur pour les 12 mélanges. Le lubrifiant possédant la CST la plus élevée avec le R134a a montré le transfert de chaleur le plus élevé : 100 % ± 20 % plus élevé que celui de R134a pur. Par contre, le transfert de chaleur du mélange avec le lubrifiant possédait la viscosité la plus faible, tandis que la CST la plus faible avec le R134a étaient de 55 % ± 9 % inférieure à celle de R134a pur. On a considéré que les films aux vitesses les plus élevées lors de l'ébullition libre du frigorigène pur ou des mélanges reflétaient l'effet du lubrifiant sur l'ébullition libre.

Mots clés : Frigorigène ; R134a ; Ébullition libre ; Transfert de chaleur ; Lubrifiant ; Concentration ; Miscibilité ; Viscosité

Nomenclature

A	surface area (m^2)
c	molar concentration of the solute
C	regression constant [Eq. (1)]
k	thermal conductivity (W/m^2 K)
L_y	length of test surface in y-direction (m)
Pr	liquid Prandtl number
q''	average wall heat flux (W/m^2)
R	universal gas constant (8.314 J/K mol)
$R_{\Delta Tw}$	residual standard deviation of superheat from cubic fit (K)
T	temperature (K)
T_i	plate–solder interface temperature (K)
T_w	temperature of surface at root of fin (K)
U	expanded uncertainty for 95% confidence
x	test surface coordinate, Fig. 2 (m)
x_m	lubricant mass fraction
y	test surface coordinate, Fig. 2 (m)

Greek symbols

Γ	surface excess concentration of solute
δ	thermal boundary layer thickness (m)
σ	surface tension ($kg/m\ s^2$)
ΔT_s	wall superheat: $T_w - T_s$ (K)
ν	viscosity (m^2/s)

Subscripts

c	lubricant critical solution temperature
e	excess layer interface
L	lubricant
ls	liquid–solid interface
m	mixture
p	pure R134a
r	refrigerant
s	saturated liquid or vapor state, solder

1. Introduction

The ability to predict the effect of lubricant on the pool boiling heat transfer of refrigerants based on the properties of the lubricant has been elusive for some time. Heat exchanger designers are interested in knowing how lubricant/refrigerant phase separation, lubricant viscosity, and lubricant mass fraction affect the performance of the evaporator. Modeling of refrigerant/lubricant mixture pool boiling has two main obstacles. First, it must be determined what lubricant properties are important and how they influence heat transfer. Second, a mechanistic model that physically represents the way a lubricant interacts with a refrigerant in the determination of heat transfer must be developed. Most of the work in refrigerant/lubricant mixture pool boiling has been done with these goals in mind.

For example, Sauer et al. [1] believed that lubricant viscosity and surface-tension effects were important in determining the magnitude of the nucleate boiling of refrigerants, but they could not correlate these effects. Hahne and Noworyta [2] also presumed that the lubricant viscosity should have an effect on pool boiling of refrigerant/lubricant mixtures, but they were unable to include it in their heat transfer correlation.

Another important parameter for pool boiling is the lubricant mass fraction. For instance, the effect of lubricant on the pool boiling performance of a Turbo-BII™ tube for R114, R124, and R123 has been investigated by Memory et al. and Webb and McQuade, respectively [3–5]. Although improvements in heat transfer with the addition of lubricant were measured by Memory et al. [3,4] for finned tubes, only degradations in heat transfer were measured for the refrigerant/lubricant mixtures and the Turbo-BII™ tube. In both of the Memory et al. [3,4] studies, they also found that for lubricant mass fractions greater than 6%, increases in lubricant concentration led to decreases in heat transfer. Bell et al. [6] found that this decrease was greater than would be expected based on mole fraction weighting.

Although no studies investigating the effect of lubricant miscibility on heat transfer were found, several

works correlate the lubricant effect to the properties of the refrigerant/lubricant mixture. For example, Jabardo and da Silva [7] developed a model for the pool boiling of R11, R113 and R114 lubricant mixtures by correlating the Rohsenow [8] surface/liquid parameter to the bubble Stanton number and to the Jakob number for each refrigerant/lubricant mixture. Another study by Chongrungreong and Sauer [9] developed a correlation for the pool boiling heat transfer of refrigerant/lubricant mixtures based on the refrigerant volume fraction and the mixture liquid Prandtl number.

Many researchers hypothesize that foaming is the main governing heat transfer mechanism for refrigerant/lubricant mixtures. Stephan [10] was one of the first researchers to connect foaming and refrigerant/lubricant evaporation and to note that an oil-rich layer exists near the tube wall. Memory et al. [3,4] also attributed the enhancement of refrigerant pool boiling heat transfer with lubricants to lubricant foaming. Other models, such as those by Jensen and Jackman [11] and Mitrovic [12], focus on the lubricant-rich layer that exists around the liquid–vapor interface of the bubble. Yet, Burkhardt and Hahne [13] believed that the influence of lubricant on pool boiling cannot be completely explained by liquid–vapor surface tension effects or by foaming.

The mechanistic model that is endorsed in this paper was developed in a series of studies [14–17]. In these studies, it was speculated that the pool boiling enhancement/degradation mechanism associated with the addition of a lubricant to refrigerant is due to an accumulation of lubricant at the boiling surface. The enhancement mechanism of lubricants is analogous to the action of surfactants in that both enhancements arise from the creation of an excess layer. Kedzierski [16] measured a significant enhancement of R123 pool boiling with the addition of 1 and 2% hexane by mass to R123. He used the Gibbs adsorption equation [18] and the Young and Dupre equation [19] to speculate that the boiling heat transfer enhancement of R123 by the addition of hexane was caused by an accumulation of hydrocarbon at the boiling surface. In essence, the greater concentration of hydrocarbon or "excess layer" at the heat transfer surface caused a reduction of the surface energy between the solid surface and the liquid. The existence of an excess layer at the liquid–solid interface is analogous to the existence of a surfactant-induced excess layer at a liquid–vapor interface. Consequently, hydrocarbons and lubricants are not typical surfactants because they accumulate at the solid–liquid interface rather than at the liquid–vapor interface. However, the reduction in the liquid–solid surface energy results in a similar reduction in bubble departure diameter that occurs with a conventional surfactant. As a consequence of the bubble size reduction, the active site density increases. A heat transfer enhancement exists when a favorable balance between an increase in site density and a reduction in bubble size occurs.

To build upon the above mechanistic model, the influence of lubricant properties on the pool boiling heat transfer must be determined. Toward this end, the boiling behavior of R134a on a Turbo-BII^{TM}-HP surface with four different polyolester lubricants (POEs) of three difference mass fractions under 4% was investigated. Table 1 gives the viscosity of the lubricants at 313.15 K: 4.59, 21.76, 25.34, and 197.36 $\mu m^2/s$. Table 1 also gives the three different critical solution temperatures (CSTs) of the R134a/lubricant mixtures that were investigated: 203, 237 and 270 K. The mixtures of this study separate into two liquid phases for temperatures less than the CST, and are completely miscible for temperatures greater than the CST. That is to say, all of the lubricants are completely miscible with R134a at the test temperature with the exception of DE589. The viscosities and CSTs of the lubricants cover the application range for refrigeration and air-conditioning equipment. Low viscosity lubricants are typically used with R134a home appliances. Screw compressors require high viscosity lubricants. Most refrigeration and air-conditioning applications require lubricants that are miscible with the refrigerant, but some applications permit the lubricant to be partially miscible with R134a.

Typically, the lubricant viscosity and its miscibility with the refrigerant are interesting in terms of how they influence the return of the lubricant to the compressor. This study shows that the very properties that favor oil return promote poor pool boiling heat transfer. Namely, a lubricant with a low viscosity and a complete miscibility with the refrigerant may promote lubricant return [20], but these characteristics are detrimental to heat transfer. Because of lubricant return concerns, Didion [21] states that a "lubricant crisis" could exist if the new lubricants are less soluble in the new refrigerants. However, the heat transfer benefit that can be obtained with the high viscosity and partially miscible lubricants may represent an opportunity rather than a crisis where lubricant return is not a problem or where it can be achieved by other means. In this way, manufacturers may be able to choose a lubricant that satisfies

Table 1
Properties of test lubricants [36]

Tableau 1
Propriétés des lubrifiants étudiés [36]

Lubricant	Viscosity at 313.15 K ($\mu m^2/s$)	Critical solution temperature (K)	Miscible in R134a (?)
DE589	21.76	270.15	Partially
DE599	4.59	203.15	Yes
DE590	25.34	237.15	Yes
DE601	197.36	203.15	Yes

the lubricating requirements of the compressor and also enhances the heat transfer of the evaporator.

2. Apparatus

Fig. 1 shows a schematic of the apparatus that was used to measure the pool boiling data of this study. Specifically, the apparatus was used to measure the liquid saturation temperature (T_s), the average pool-boiling heat flux (q''), and the wall temperature (T_w) of the test surface at the root of the fin. The three principal components of the apparatus were test chamber, condenser, and reservoir. The internal dimensions of the test chamber were 25.4 mm × 257 mm × 1.54 m. The test chamber was charged with approximately 7 kg of R134a from the reservoir, giving a liquid height of approximately 80 mm above the test surface. As shown in Fig. 1, the test section was visible through two opposing, flat 150×200 mm quartz windows. A high-speed camera was used to film the boiling at 1000, 3000, and 6000 frames per second (fps). Two 500 W forward lights illuminated the specimens during filming. Films were taken at selected heat fluxes immediately after the measurement of the heat-transfer coefficient to ensure that the heat from the lights did not influence the measurement. The bottom of the test surface was heated with high velocity (2.5 m/s) water flow. The vapor produced by liquid boiling on the test surface was condensed by the brine-cooled, shell-and-tube condenser and returned as liquid to the pool by gravity.

To reduce the errors associated with the liquid saturation temperature measurement, the saturation temperature of the liquid was measured with a 450 mm long, 1.6 mm diameter stainless steel sheathed thermocouple. The small diameter provided for a relatively rapid response time. To minimize conduction errors, nearly the entire length of the thermocouple was in contact with either the test refrigerant vapor or liquid. The tip of the thermocouple was placed approximately 2 mm above and 150 mm to one side of the top of the test surface. This placement ensured that approximately 80 mm of the probe length was in relatively well-mixed liquid near the two-phase fluid above the test surface. To provide for a saturated liquid pool state, the mass of liquid in the pool was large compared to the mass of liquid condensed. At the highest heat flux, nearly 1 hour was required to evaporate and condense the entire test chamber charge. The lack of a temperature difference between the probe and the well-insulated, low emissivity, 38 mm aluminum test chamber walls essentially eliminated temperature errors due to radiation to the probe.

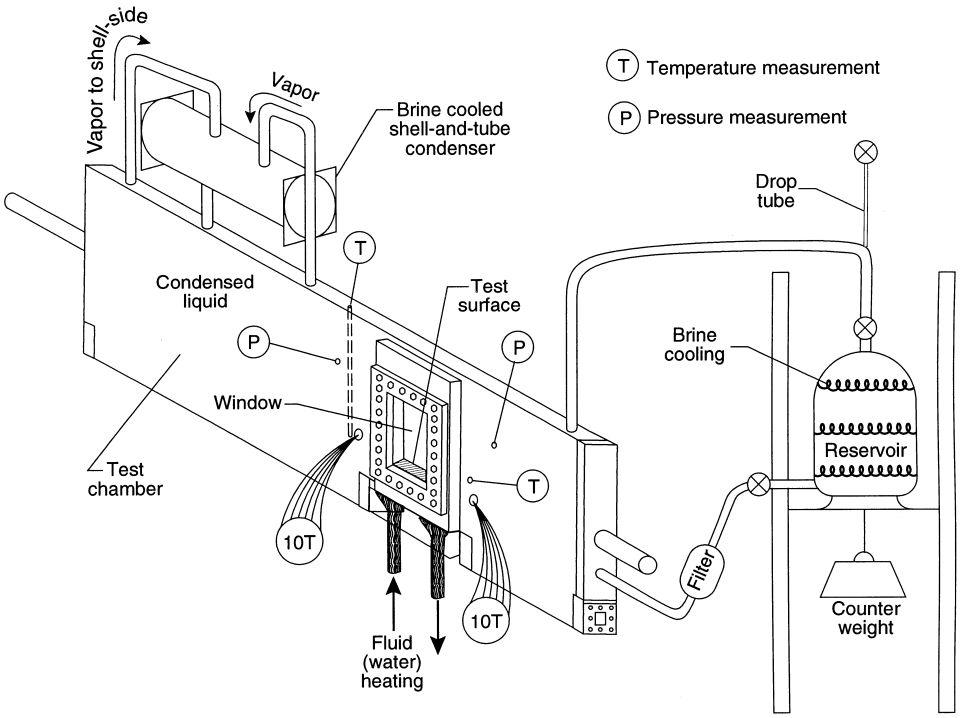

Fig. 1. Schematic of test apparatus.

Fig. 1. Schéma de l'installation expérimentale.

3. Test surface

Fig. 2 shows the oxygen-free high-conductivity (OFHC) copper Turbo-BII^{TM}-HP test plate and thermocouple coordinate system used in this study. Commercially, the Turbo-BII^{TM}-HP surface is formed by a rolling process on a smooth copper tube. The test plate was machined out of a single piece of OFHC copper by electric discharge machining (EDM). The Turbo-BII^{TM}-HP surface in this study was flattened from a 25 mm OD annealed copper tube and soldered onto the top of the test plate. Fig. 3 shows a photograph of the fin surface. The Turbo-BII^{TM}-HP surface has approximately 2250 fins per meter (fpm) oriented along the short axis of the plate. A canopy of copper diamonds merge to create 0.1 mm wide (approximately) slit openings to the root of the fin ranging from approximately 0.1 to 0.3 mm in length. The overall height and root-width of a fin are 0.8 and 0.2 mm, respectively.

4. Measurements and uncertainties

The standard uncertainty (u_i) is the positive square root of the estimated variance u_i^2. The individual standard uncertainties are combined to obtain the combined standard uncertainty (u_c) by the law of propagation of uncertainty. The u_c becomes an expanded uncertainty (U) when it is multiplied by a coverage factor to correspond to a particular confidence interval. All of the measurement uncertainties reported in this document are expanded uncertainties (U) for a 95% confidence interval except where specified otherwise.

The thermocouples were calibrated against a standard in the NIST Temperature Group to a residual standard deviation of 0.005 K. Considering the fluctuations in the saturation temperature during the test and the standard uncertainties in the calibration, the u_c of the average saturation temperature was no greater than 0.04 K. A thermocouple drift of within 0.1 K was determined by recalibrating the thermocouples a year after the tests were completed. Consequently, the u_c of the temperature measurements was less than 0.1 K.

Fig. 2 shows the coordinate system for the 20 wells where individual thermocouples were force-fitted into the side of the test plate. The wells were 16 mm deep to reduce conduction errors. Using a method given by Eckert and Goldstein [22], errors due to heat conduction along the thermocouple leads were estimated to be well below 0.01 mK. The origin of the coordinate system was

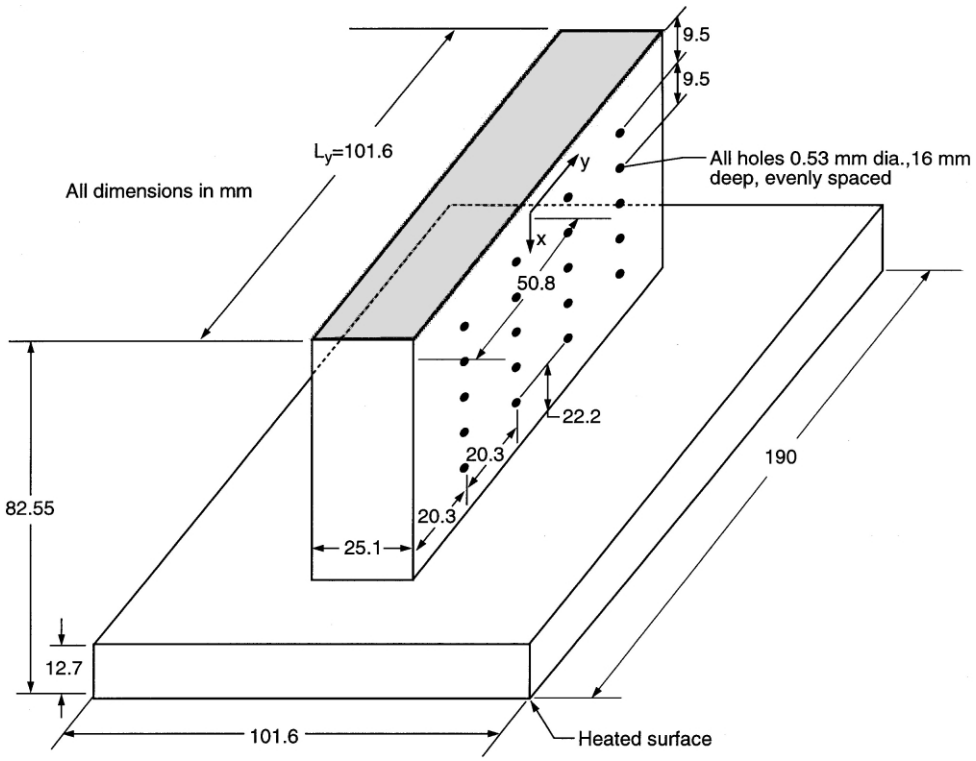

Fig. 2. OFHC copper Turbo-BII^{TM}-HP test plate and thermocouple coordinate system.

Fig. 2. Plaque d'essai hautement conductrice dépourvue d'oxygène (OFHC) en cuivre TurboBII^{TM}-HP et système de coordonnées à thermocouple.

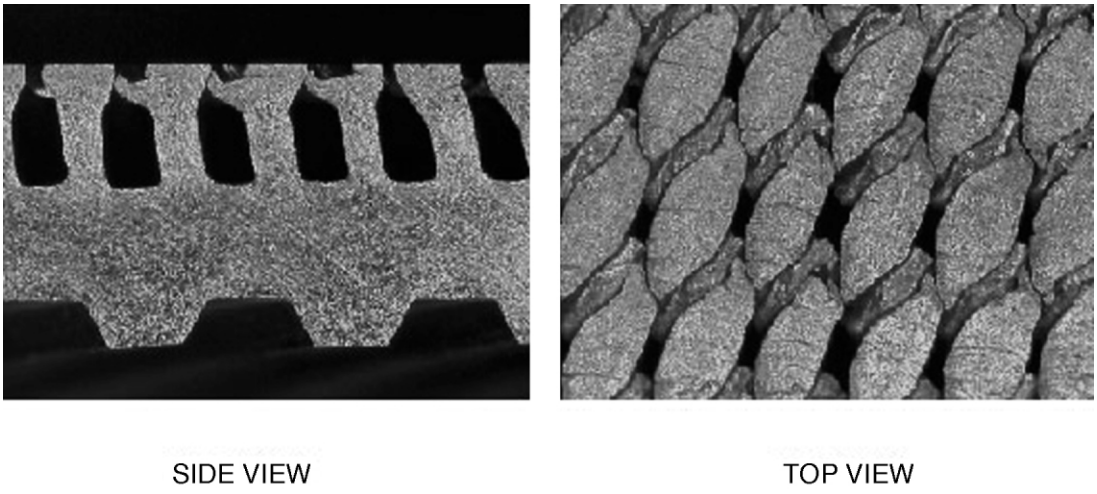

Fig. 3. Photograph of Turbo-BII™-HP surface with all dimensions in millimeters.

Fig. 3. Photo de la surface Turbo-BII™-HP avec les dimensions exprimées en mm.

centered on the surface with respect to the y-direction at the plate surface–solder layer interface. Centering the origin in the y-direction improved the accuracy of the wall heat flux and temperature calculations by reducing the number of fitted constants involved in these calculations. The x-coordinate measures the distance normal to the heat transfer surface. The y-coordinate measures the distance perpendicular to the x-coordinate. The thermocouples were arranged in four sets of five aligned in the x-direction. Following a procedure given by Kedzierski and Worthington [23], the size and arrangement of the thermocouple wells were designed to minimize the errors in the wall temperature and temperature gradient measurement.

The heat flux and the wall temperature were obtained by regressing the measured temperature distribution of the copper plate to the governing two-dimensional conduction equation (Laplace equation). In other words, rather than using the boundary conditions to solve for the interior temperatures, the interior temperatures were used to solve for the boundary conditions following a backward stepwise procedure given in Kedzierski [24].

The backward stepwise regression was used to determine the best model or the significant terms of the solution to the Laplace equation in rectangular coordinates for each data point. Most infinite series solutions should converge within nine terms. The backward stepwise method began by regressing the first nine terms of the infinite series solution to the 20 measured plate temperatures:

$$\begin{aligned} T = {} & C_0 + C_1 x + C_2 y + C_3(x^2 - y^2) + 2C_4 xy \\ & + C_5 x(x^2 - 3y^2) + C_6 y(3x^2 - y^2) \\ & + C_7(x^4 - 6x^2y^2 + y^4) + 4C_8(x^3 y - xy^3) \end{aligned} \tag{1}$$

The above "full" model was reduced to its significant terms by removing terms with t-values less than 2 while maintaining the original residual standard deviation of the full model. Terms were removed one at a time. Regression of the 20 temperatures was done after each term with the smallest t-value was removed.

Fourier's law and the fitted constants ($C_0, C_1, \ldots C_n$) were used to calculate the average heat flux (q'') normal to and evaluated at the heat transfer surface, e.g.:

$$q'' = \left(\frac{1}{L_y} \int_{\frac{-L_y}{2}}^{\frac{L_y}{2}} k \frac{\partial T}{\partial x} \mathrm{d}y \right)_{x=0} = \bar{k} C_1 \tag{2}$$

where $\bar{k}$ is the average thermal conductivity along the surface of the plate, and L_y is the length of the heat transfer surface, as shown in Fig. 2.

The average plate–solder layer interface temperature (T_i) was calculated by integrating the local temperature of the heat surface just below the solder layer that attached the Turbo-BII™-HP tube to the test surface:

$$T_i = \left(\frac{1}{L_y} \int_{-\frac{L_y}{2}}^{\frac{L_y}{2}} T \mathrm{d}y \right)_{x=0} \quad (3)$$

For most models, the above equation reduces to:

$$T_i = C_0 \quad (4)$$

A linear conduction model was used to calculate the heat transfer across the solder layer and the average wall temperature at the root of the fin (T_w). The procedure that was used to extrapolate the wall temperature of the surface while accounting for the solder layer and the thickness of the tube at the fin root is discussed in Kedzierski [25]. The correction for the solder layer adds approximately 0.004 K to the expanded uncertainty of T_w. The expanded uncertainty of T_w was calculated from the regression of the solution to Laplace's equation. The mean uncertainties in the wall temperature for the five fluids range from approximately 0.03 K at 5 kW/m^2 to 0.09 K at 160 kW/m^2. The average random error in the wall temperature difference — $\Delta T_s = T_v - T_w$ — for all of the fluids was within 0.07 K for heat fluxes less than 80 kW/m^2.

Siu et al. [26] estimated the expanded uncertainty in the thermal conductivity of OFHC copper to be about 2 to 3% by comparing round-robin experiments. Considering this, the relative expanded uncertainty in q'' was greatest at the lowest heat fluxes, being between 3 and 10% for heat fluxes less than 10 kW/m^2. In general, the $E_{q''}$ appears to remain between 2.8 and 4% for heat fluxes greater than 30 kW/m^2. A more detailed discussion of the uncertainty analysis can be found in Kedzierski [25].

The test rig and the test surface were thoroughly cleaned after each lubricant mixture was tested. A checkout test followed, which confirmed that the rig was clean by reproducing the pure R134a data. If the checkout test did not reproduce the pure R134a results within 3%, the rig and surface were cleaned again, and the test was repeated.

5. Pool boiling measurements

The heat flux was varied from approximately 10 to 160 kW/m^2. This test range includes the operating conditions of R134a chillers equipped with enhanced tubes. All evaporation tests were taken at a saturation temperature of 277.6 K. The data were consecutively recorded starting at approximately 160 kW/m^2 and then descending to 10 kW/m^2. The descending heat flux procedure minimized the possibility of any hysteresis effects on the data, which would have made the data sensitive to the initial operating conditions. The measured heat flux and wall superheat for all of the data of this study are tabulated in Kedzierski [25]. On average, 9 days of data or approximately 165 data points were taken for each fluid.

The mixtures were prepared by first charging approximately 90% of a known mass of R134a into an evacuated reservoir (see Fig. 1). The liquid was injected into a drop tube that nearly touched the bottom of the reservoir. For the near 0.5% composition, the lubricant was first injected with a syringe through the drop tube. Next, the drop tube was flushed with the remaining R134a charge. For the remaining two lubricant compositions, additional lubricant was injected with the aid of R134a as a propellant. The flushing of R134a propellant vapor through the drop tube also assisted in sample mixing. The mass fraction was determined from the masses of the charged components. Three nominal lubricant mass fractions were investigated: 0.5, 1, and 2%. The expanded uncertainty of the mass fraction measurement for plus or minus three standard deviations was approximately 0.02%, e.g. the range of a 0.5% composition was between 0.48 and 0.52%. The DE601, DE590, and DE599 mixtures with R134a have a greater uncertainty of approximately ±0.06% for the two highest concentrations. The heat-transfer test chamber was charged with the test fluid from the reservoir before each day of testing.

Fig. 4 is a plot of the measured heat flux (q'') versus the measured wall superheat ($T_w - T_s$) for pure R134a at $T_s = 277.6$ K. Symbols represent the data points. The solid line is a best-fit regression or estimated mean of the data. A single cubic fit was used to regress the wall superheat against the heat flux for the entire heat flux range. Table 2 gives the constants for the cubic regression for each test fluid. Fig. 5 plots the cubic fits for all of the test fluids on logarithmic scales. The residual standard deviation of the regressions — representing the proximity of the data to the mean — are given in Table 3. On average, the residual standard deviation of the pure R134a and the (99.5/0.5) mixture data about the mean was approximately 0.1 K. Fig. 6 shows that the residual standard deviation of the cubic fit increases approximately linearly with respect to lubricant mass fraction for each lubricant except DE589. The dashed lines to either side of the mean represent the lower and upper 95% simultaneous (multiple-use) confidence intervals for the mean. The expanded uncertainty of the estimated mean wall superheat for pure R134a and the (99.5/0.5) mixtures, the (99/1) mixtures and the (98/2) mixtures was on average 0.05, 0.1, and 0.16 K, respectively. Table 4 provides the average mean wall temperature expanded uncertainty for all of the fluids.

Because of the random trends of the cubic fit residual plots, the increase in the lack of reproducibility with increasing concentration shown in Fig. 6 is believed to be caused by a true physical phenomenon. Apparently

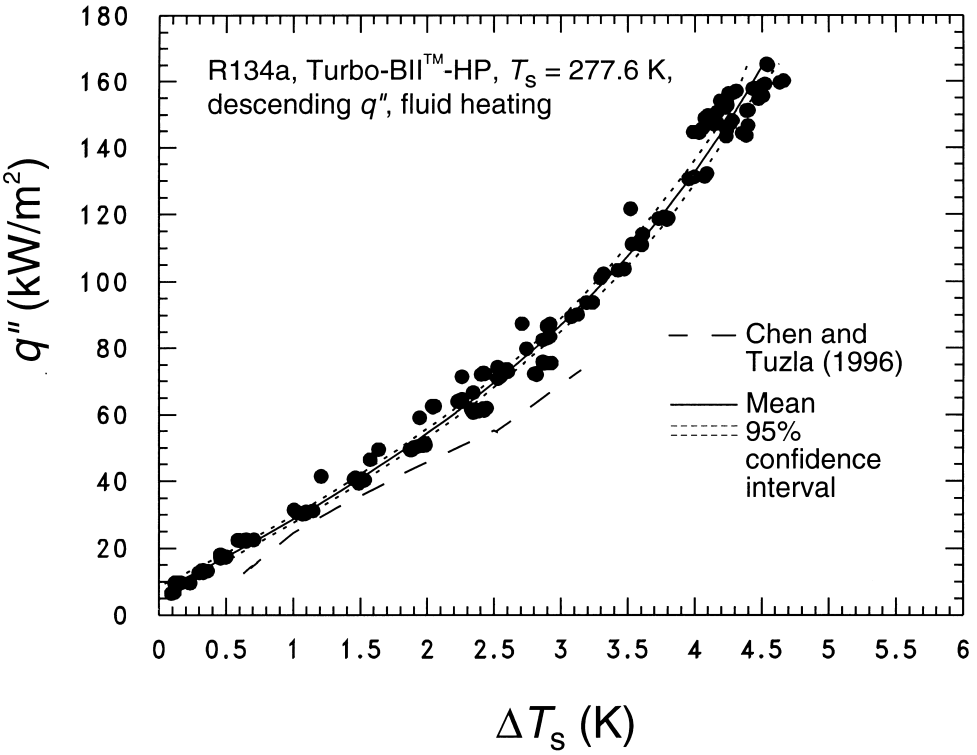

Fig. 4. Pure R134a boiling curve for Turbo-BII^{TM}-HP.

Fig. 4. Courbe d'ébullition de R134a pur pour la surface Turbo-BII^{TM}-HP.

Table 2
Constants for cubic boiling curve fits for Turbo-BII^{TM}-HP[a]

Tableau 2
Constantes des courbes d'ébullition pour la surface Turbo-BII^{TM}-HP

Fluid	A_o	A_1	A_2	A_3
R134a/DE589 (99.5/0.5) $\Delta T_s \leqslant 4.8$ K	−0.552305	4.40522×10^{-5}	-5.58725×10^{-11}	-8.33712×10^{-17}
R134a/DE589 (99/1) $\Delta T_s \leqslant 4.9$ K	−0.0785764	3.18519×10^{-5}	2.91081×10^{-11}	-2.39599×10^{-16}
R134a/DE589 (98/2) $\Delta T_s \leqslant 4.4$ K	−0.0545181	4.07832×10^{-5}	-4.07832×10^{-11}	-2.04793×10^{-16}
R134a/DE590 (99.5/0.5) $\Delta T_s \leqslant 4.5$ K	−0.382810	3.89896×10^{-5}	2.10968×10^{-11}	-4.48145×10^{-16}
R134a/DE590 (98.8/1.2) $\Delta T_s \leqslant 5.0$ K	−0.459516	5.35886×10^{-5}	-1.50659×10^{-10}	1.65968×10^{-16}
R134a/DE590 (97.3/2.7) $\Delta T_s \leqslant 5.0$ K	0.273636	2.53193×10^{-5}	3.83839×10^{-10}	-2.13652×10^{-15}
R134a/DE599 (99.5/0.5) $\Delta T_s \leqslant 4.9$ K	0.384319	1.69417×10^{-5}	2.55120×10^{-10}	-1.15269×10^{-15}
R134a/DE599 (98.9/1.1) $\Delta T_s \leqslant 5.3$ K	0.377557	2.66641×10^{-5}	1.69317×10^{-10}	-9.03561×10^{-16}
R134a/DE599 (97.7/2.3) $\Delta T_s \leqslant 6.4$ K	0.0441903	8.54216×10^{-5}	-3.88627×10^{-10}	6.57693×10^{-16}
R134a/DE601 (99.5/0.5) $\Delta T_s \leqslant 5.1$ K	−0.546989	4.36860×10^{-5}	4.66413×10^{-12}	-3.67216×10^{-16}
R134a/DE601 (98.7/1.3) $\Delta T_s \leqslant 5.4$ K	−0.540402	4.52935×10^{-5}	2.49306×10^{-11}	-4.98398×10^{-16}
R134a/DE601 (96.7/3.3) $\Delta T_s \leqslant 6.0$ K	−0.444023	7.13944×10^{-5}	-3.01331×10^{-10}	6.46025×10^{-16}
R134a $\Delta T_s \leqslant 4.5$ K	−0.360766	5.28759×10^{-5}	-1.88076×10^{-10}	2.81359×10^{-16}

[a] $\Delta T_s = A_0 + A_1 q'' + A_2 q''^2 + A_3 q''^3 \Delta T_s$ in Kelvin and q'' in W/m^2.

for some R134a/lubricant mixtures, larger bulk lubricant concentrations can lead to greater variability in the data from day-to-day, which leads to a spreading of the data. A possible explanation for the sensitivity of the data is that higher bulk concentrations exhibit a greater day-to-day variation in the bubble size and site density. The variation in the bubble parameters is likely linked directly to the between-run variation in the concentra-

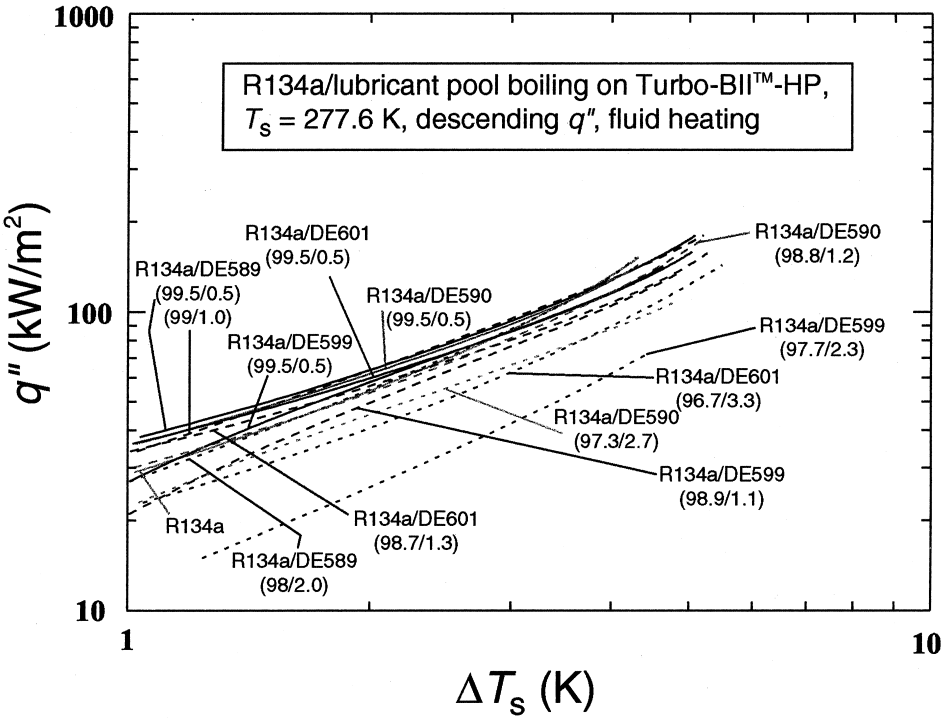

Fig. 5. Pool boiling curves for R134a and 12 R134a/lubricant mixtures on Turbo-BII™-HP.

Fig. 5. Courbes d'ébullition de R134a et des mélanges de R134a/lubrifiant pour la surface Turbo-BII™-HP.

Table 3
Residual standard deviation of ΔT_s from the mean

Tableau 3
Ecart type résiduel ΔT_s par rapport à la moyenne

Fluid	U *(K)*
R134a/DE589 (99.5/0.5)	0.09
R134a/DE589 (99/1)	0.10
R134a/DE589 (98/2)	0.10
R134a/DE590 (99.5/0.5)	0.11
R134a/DE590 (98.8/1.2)	0.33
R134a/DE590 (97.3/2.7)	0.64
R134a/DE599 (99.5/0.5)	0.11
R134a/DE599 (98.9/1.1)	0.16
R134a/DE599 (97.7/2.3)	0.40
R134a/DE601 (99.5/0.5)	0.08
R134a/DE601 (98.7/1.3)	0.20
R134a/DE601 (96.7/3.3)	0.28
R134a	0.11

tion of the lubricant excess layer at the surface. This suggests that the variation in the lubricant concentration at the surface may be greater for higher bulk concentrations and result in a greater variation in the heat transfer. Considering the absence of site density and bubble size data for the entire heat flux range and a model to relate these bubble parameters to the heat flux, a simple cubic fit provided an unbiased means for comparison of all the data.

The R134a pool boiling data of Chen and Tuzla [27] on a 19 mm OD Turbo-BII™-HP tube at $T_s = 277.6$ K is compared to the present data in Fig. 4. The Chen and Tuzla [27] wall superheat is anywhere from 0.2 to 0.5 K greater than the mean wall superheat of the NIST data for a given heat flux. Although flattening the Turbo-BII™-HP tube did not appear to alter the fin structure, the process may have affected the heat transfer performance. Also, significant differences in heat transfer for Turbo-BII™-HP tubes can exist even though they have been formed by the same tooling [28]. Differences in heat transfer performance between the flat plate and the round tube arise primarily from differences in the bulk fluid motion and the conduction experienced by the two surfaces. Bulk fluid motion, including the sliding bubble effect [29], should cause the tube performance to be greater than that of the flat plate. Conduction effects should be small for the copper tube and plate. As a consequence, the proximity of the two data sets suggests that either: (1) there are compensating effects between, for example, the heat transfer enhancement by bulk fluid motion and measurement errors for the tube and/

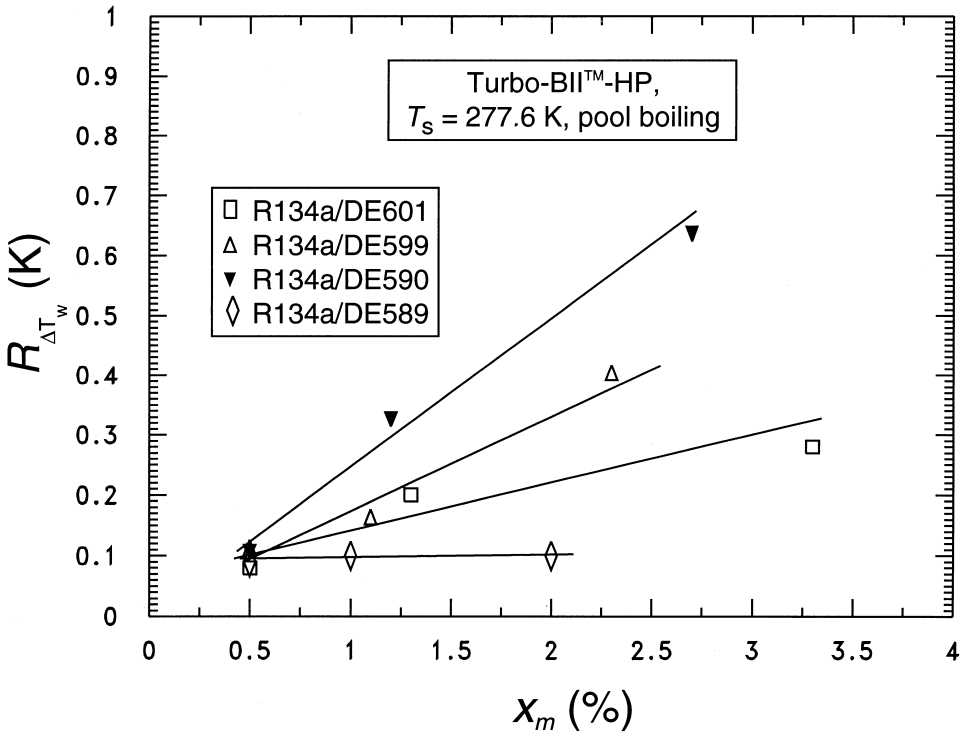

Fig. 6. Effect of lubricant mass fraction on residual standard deviation of cubic fit.

Fig. 6. Effet de la fraction massique sur l'écart type résiduel.

Table 4
Average magnitude of 95% multi-use confidence interval for mean $T_w - T_s$ (K)

Tableau 4
Grandeur moyenne de l'intervalle de confiance à 95% pour la moyenne $T_w - T_s$ (K)

Fluid	U (K)
R134a/DE589 (99.5/0.5)	0.048
R134a/DE589 (99/1)	0.058
R134a/DE589 (98/2)	0.056
R134a/DE590 (99.5/0.5)	0.055
R134a/DE590 (98.8/1.2)	0.155
R134a/DE590 (97.3/2.7)	0.252
R134a/DE599 (99.5/0.5)	0.052
R134a/DE599 (98.9/1.1)	0.088
R134a/DE599 (97.7/2.3)	0.192
R134a/DE601 (99.5/0.5)	0.046
R134a/DE601 (98.7/1.3)	0.103
R134a/DE601 (96.7/3.3)	0.157
R134a	0.058

or random differences in the fin structure between the plate and the tube, or (2) the bulk fluid motion has only a minimal affect on the heat transfer performance of the enhanced tube. Possibly, the fin canopies of the Turbo-BII™-HP shelter the nucleate boiling from the bulk fluid motion causing the boiling to be independent of the fluid motion. In any case, it appears that the flat test surface provides a fair representation of the performance of a tube but with the advantage of significantly smaller measurement uncertainties.

6. Enhancement trends

Figs. 7–10 summarize the effect of adding lubricant to R134a on the R134a heat flux. Each figure plots the ratio of the mixture heat flux (q''_m) to the pure R134a heat flux (q''_p) versus the pure R134a heat flux at the same wall superheat. The 95% confidence interval for the heat flux ratio is depicted as a shaded region in the figures. Larger uncertainties in the q'' measurement and larger uncertainties in the fit of the data result in larger confidence intervals at low heat flux.

In general, a boiling enhancement occurs for the 0.5% lubricant mass fraction for all of the refrigerant/lubricant mixtures that were tested. For the most part, the mixture heat flux diminishes with increasing lubricant mass fraction. The rate of degradation with increasing mass fraction is less severe for mixtures with the DE589 lubricant. Also, no enhancement occurs for the 2%

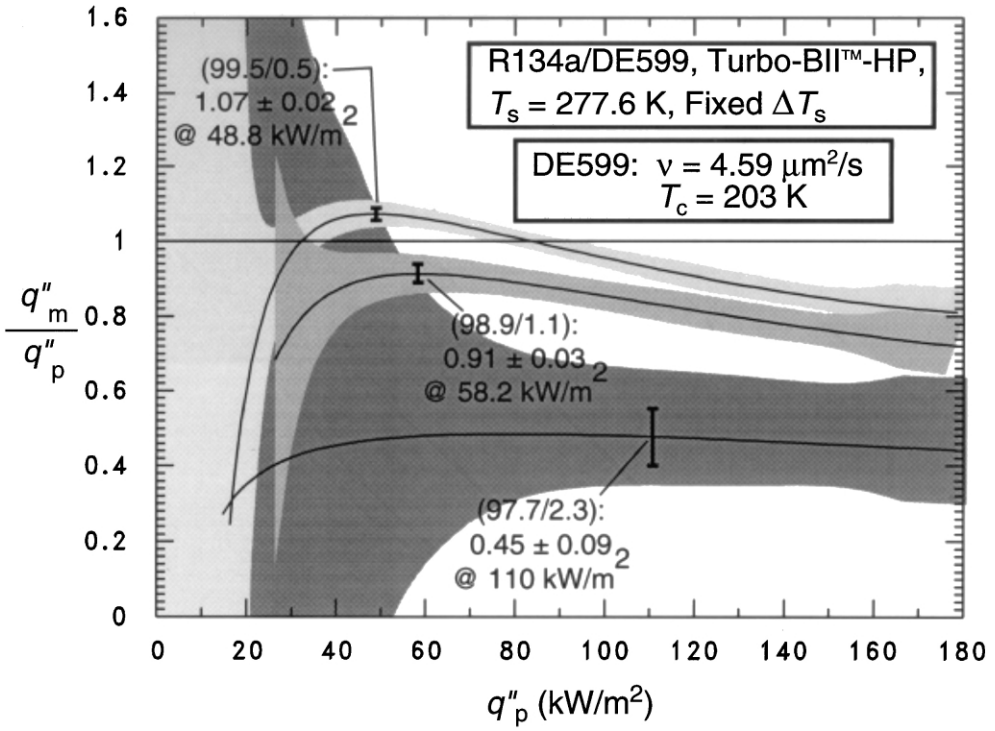

Fig. 7. R134a/DE599 mixtures heat flux relative to that of pure R134a.

Fig. 7. Flux thermiques des mélanges de R134a/DE599 comparés à celui de R134a pur.

lubricant concentration for any of the mixtures. In addition, the heat transfer for all of the R134a/lubricant mixtures decreases with respect to increasing heat flux for heat fluxes greater than 60 kW/m^2. Although the heat flux ratio is shown to increase with heat flux in some regions, the corresponding uncertainties in the heat flux ratio are too large to confirm that trend.

Fig. 7 shows the heat flux ratio for three mixtures of R134a and the DE599 lubricant. The viscosity of the DE599 lubricant is the smallest of the four lubricants (4.6 μm^2/s at 313 K), and it is miscible with R134a at the test temperature. For the most part, the R134a boiling was not enhanced by the addition of DE599. The sole improvement in the heat transfer was an average 3% increase in the heat flux between approximately 30 and 80 kW/m^2 for the (99.5/0.5) mixture. In addition, the R134a/DE599 (97.7/2.3) mixture exhibited the greatest degradation in heat transfer; the heat flux ratio was approximately 0.45±0.09 for the entire heat flux range. The greatest heat flux ratio exhibited by the R134a/DE599 (98.9/1.1) mixture was 0.91±0.03 at 58.2 kW/m^2.

Fig. 8 shows the heat flux ratio for three mixtures of R134a and the DE601 lubricant. The viscosity of the DE601 lubricant is the greatest of the four lubricants (197.36 μm^2/s at 313 K), and it has the same CST as the DE599 lubricant with R134a (203 K). Two mixtures of DE601 with R134a (99.5/0.5 and 98.7/1.3) exhibit a substantial enhancement within the operating range of R134a chillers. Specifically, a 16 and a 9% average enhancement of the pure R134a heat flux were obtained between approximately 14 and 81 kW/m^2. The two greatest heat flux ratios were 1.47±0.06 and 1.37±0.1, which were obtained at approximately 14 kW/m^2 for the (99.5/0.5), and the (98.7/1.3) mixture, respectively. The (96.7/3.3) mixture exhibits a heat transfer degradation with respect to the heat transfer of pure R134a for all heat fluxes. Performance loss due to a given increase in mass fraction was more severe when the lubricant mass fraction was increased from 1.3 to 3.3% than it was when the increase was from 0.5 to 1.3%.

Fig. 9 shows the heat flux ratio for three mixtures of R134a and the DE590 lubricant. The viscosity of the DE590 lubricant is between that of the DE601 and the DE599 lubricants (25.34 μm^2/s at 313 K), and it has a slightly higher CST (237 K) with R134a than these lubricants. The R134a/DE590 (99.5/0.5) mixture exhibits a maximum heat flux increase over that of pure R134a of 37%±14% at approximately 9 kW/m^2. The

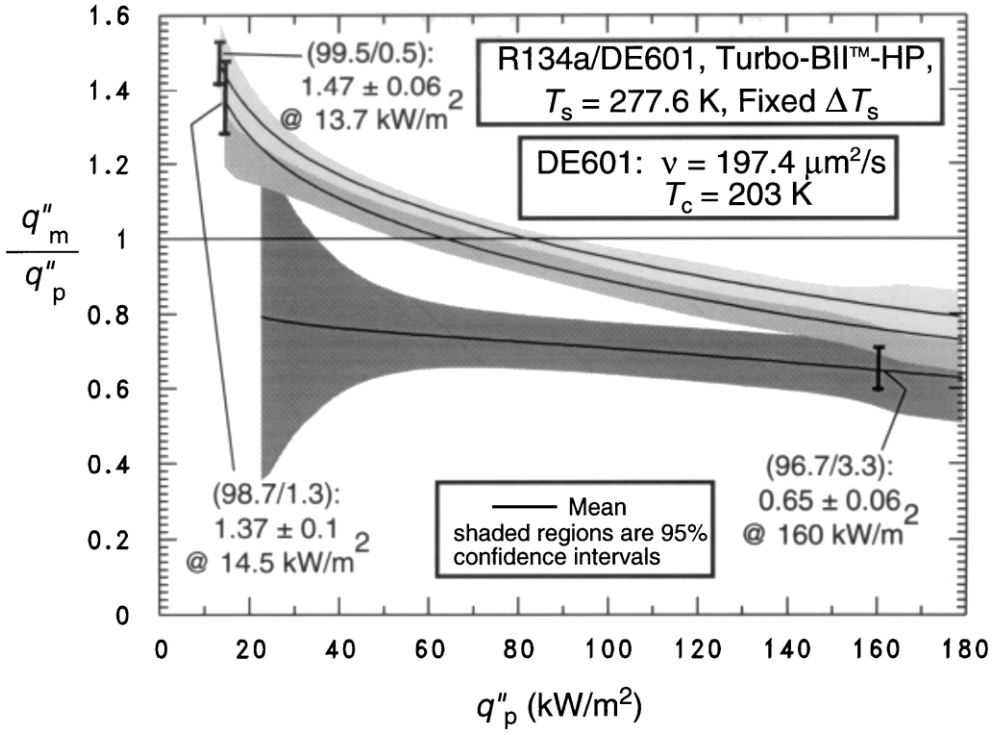

Fig. 8. R134a/DE601 mixtures heat flux relative to that of pure R134a.

Fig. 8. Flux thermiques des mélanges de R134a/DE601 comparés à celui de R134a pur.

average heat flux ratio for the R134a/DE590 (99.5/0.5) mixture is 1.18 over the heat flux range of interest to chillers — from approximately 11 to 81 kW/m^2. By contrast, the heat flux ratios of the R134a/DE590 (98.8/1.2) and the R134a/DE590 (97.3/2.7) mixtures are significantly less than that of the (99.5/0.5) mixture being 0.9±0.03 and 0.6±0.5 at 110 kW/m^2, respectively. Notice that because the confidence intervals for both the R134a/DE590 (98.8/1.2) and the R134a/DE590 (97.3/2.7) mixtures include $q''_m/q''_p = 1$ at low heat flux, the relative performance of these mixtures with respect to pure R134a is indeterminate in this region.

Fig. 10 shows the heat flux ratio for three mixtures of R134a and the DE589 lubricant. The viscosity of the DE589 lubricant is nearly the same as that of the DE590 lubricant (21.76 μm^2/s at 313 K), and it has the highest CST (270 K) with R134a of all the lubricants. Mixtures of R134a with DE589 exhibit the largest enhancements with respect to R134a and are not as sensitive to lubricant concentration as the other lubricants investigated. In fact, the 0.5 and 1% concentrations with DE589 have nearly identical performances for pure heat fluxes greater than 50 kW/m^2. The maximum heat flux ratio for R134a/DE589 (99.5/0.5) is 2.0±0.2 at approximately 5 kW/m^2. The maximum heat flux ratio for R134a/DE589 (99/1) is 1.18±0.02 at approximately 40 kW/m^2. The heat flux ratio for the 0.5 and 1% DE589 mixtures, averaged over approximately 10 and 81 kW/m^2, is 1.24 and 1.13, respectively. The 2% DE589 mixture with R134a exhibits a boiling performance approximately equal to that of pure R134a.

6.1. Regression analysis

The heat flux ratios given in Figs. 7–10 provide the heat transfer performance of the R134a/lubricant mixtures relative to that of pure R134a for each of the four R134a/lubricant sets. However, the effects of lubricant viscosity, CST (T_c), and lubricant mass fraction on the mixture heat transfer are not easily isolated nor understood with heat flux ratio plots alone. To remedy this, a regression analysis of the average heat flux ratios for each mixture versus the three salient factors and their coupling is presented. The heat flux ratios were averaged from approximately 10 to 80 kW/m^2. The regression factors were: (1) the lubricant mass fraction (x_m), (2) the difference between the liquid viscosity of the lubricant and that of the refrigerant normalized by the refrigerant

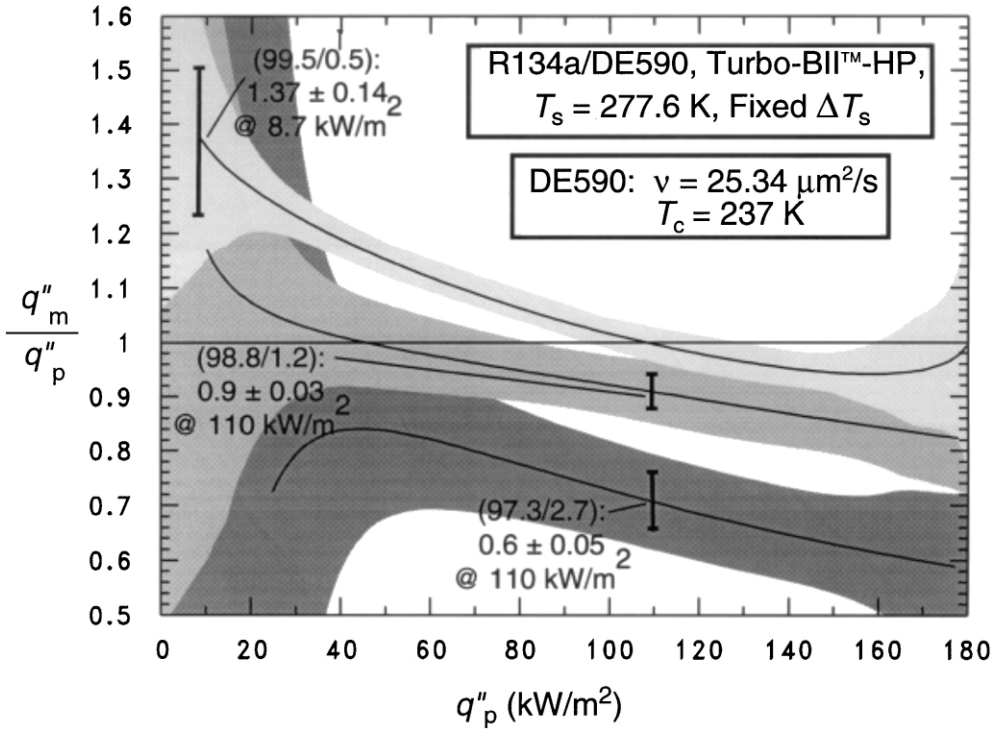

Fig. 9. R134a/DE590 mixtures heat flux relative to that of pure R134a.

Fig. 9. Flux thermiques des mélanges de R134a/DE590 comparés à celui de R134a pur.

viscosity $(\nu_L - \nu_r)/\nu_r$ all evaluated at 313 K, and (3) the difference between the saturated fluid temperature and the CST of the R134a/lubricant mixture normalized by the fluid temperature $(T_s - T_c)/T_s$. The normalized viscosity difference was evaluated at 313 K due to the lack of lubricant viscosity data at T_s. However, the use of $(\nu_L - \nu_r)/\nu_r$ at 313 K is sufficient to illustrate the relative effects of viscosity.

Fig. 11 shows a plot of the average heat flux ratio versus lubricant mass fraction for the four lubricant mixtures of this study. Clearly, the pool boiling performance decreases with respect to increasing lubricant mass fraction for each R134a/lubricant mixture. Sato et al. [30] have shown a similar pool boiling performance decrease with respect to increasing lubricant mass fraction for R134a/PAG lubricant mixtures. Because of the large variability of the data shown in Fig. 11, the lubricant mass fraction evidently does not capture the entire dependence of the heat flux ratio.

At this point, a regression analysis to determine the importance of each of the selected R134a/lubricant properties for pool boiling was done. A total of seven factors — the three salient factors listed above plus four interaction terms- were examined for their influence on the heat flux ratio. As a result, the following model of the average heat flux ratio was fitted to within ±0.1 for 95% confidence:

$$\frac{\overline{q_m}}{q_p} = 1.25 - x_m \left\{ 91.9 - \left(\frac{\nu_L - \nu_r}{\nu_r} \right) \left[0.529 - 1.92 \left(\frac{T_s - T_c}{T_s} \right) \right] - 211 \left(\frac{T_s - T_c}{T_s} \right) \right\} \quad (5)$$

Fig. 12 plots the measured heat flux ratio versus that predicted by Eq. (5). The figure illustrates that including the lubricant viscosity and the miscibility effects have nearly collapsed the data of Fig. 11 onto a single line. Eq. (5) shows that a small lubricant mass fraction, a small $(T_s - T_c)/T_s$, and a large lubricant viscosity all tend to benefit R134a/lubricant pool boiling heat transfer. The lubricant mass fraction is the most influential of the governing parameters. As compared to x_m, the lubricant viscosity and the $(T_s - T_c)/T_s$ are less important, but they are still significant for determining the magnitude of the average heat flux ratio. Notice that the lubricant viscosity parameter is coupled to the $(T_s - T_c)/T_s$ parameter. Here the $(T_s - T_c)/T_s$ parameter reduces the effect of viscosity on the heat transfer. For example, if a lubricant has a large viscosity that

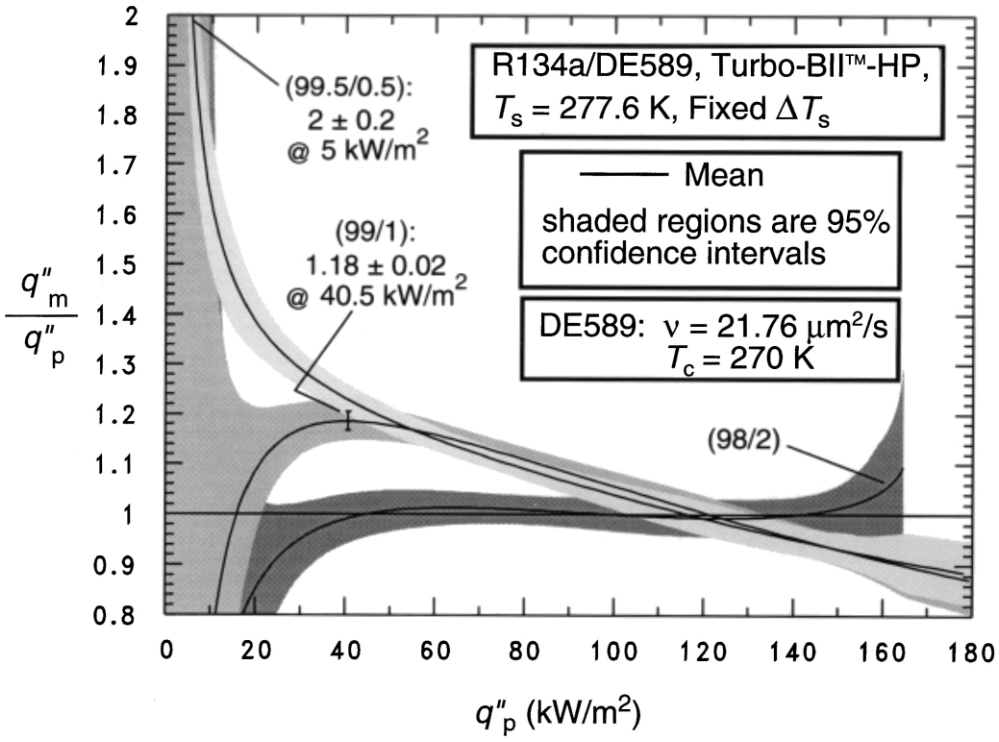

Fig. 10. R134a/DE589 mixtures heat flux relative to that of pure R134a.

Fig. 10. Flux thermiques des mélanges de R134a/DE589 comparés à celui de R134a pur.

will benefit heat transfer, but if it also has a test temperature that is far from the CST, then the viscosity enhancement effect will be somewhat lessened by the large $(T_s - T_c)/T_s$.

There are a couple of caveats that should be given with Eq. (5). First, the quantity within the outermost brackets that multiplies x_m must be greater than zero to provide for a decreasing enhancement with respect to increasing lubricant mass fraction. Otherwise, heat flux ratios of 60 at a lubricant mass fraction of 10% can be obtained for the highest lubricant viscosity and the lowest CST. For these inputs, the model predicts that the heat flux ratio increases with increasing mass fraction for mass fractions greater than 5%, which is inconsistent with current experience. However, if the viscosity and CST inputs to the model were limited such that the model produced only decreasing heat flux ratios with respect to mass fraction, then the highest possible enhancement would be approximately 25%. A limit on the enhancement also does not make physical sense. Finally, the model predicts an enhancement ratio of 1.25 rather than 1.00 for pure R134a. Consequently, the above model should only be used to illustrate the trends of the current data set for positive values of the x_m multiplier.

7. Mechanistic interpretation

The above regression analysis has shown that the viscosity, the CST, and the lubricant mass fraction are important factors for R134a pool boiling. The analysis also shows that the viscosity and the CST are coupled. The role that the lubricant mass fraction, the viscosity, and the miscibility have on R134a pool boiling can be understood by analyzing how these parameters interact with the lubricant excess layer. The lubricant excess layer exists as a region of liquid near a heated wall with a lubricant concentration that is greater than that of the bulk fluid. In the following, mechanistic interpretations are offered to explain how each of the influential factors affect R134a pool boiling.

Larger lubricant mass fractions promote smaller bubble departure diameters, which, in turn, can lead to poorer heat transfer [14,15]. As outlined by Kedzierski [17], the excess layer causes a reduction in the liquid-solid surface energy (σ_{ls}) that results in a simultaneous reduction in the bubble departure diameter and an increase in the site density. This was illustrated with the Gibbs adsorption equation for a dilute solution [18], which shows that a greater surface energy reduction results for increases in the surface excess concentration

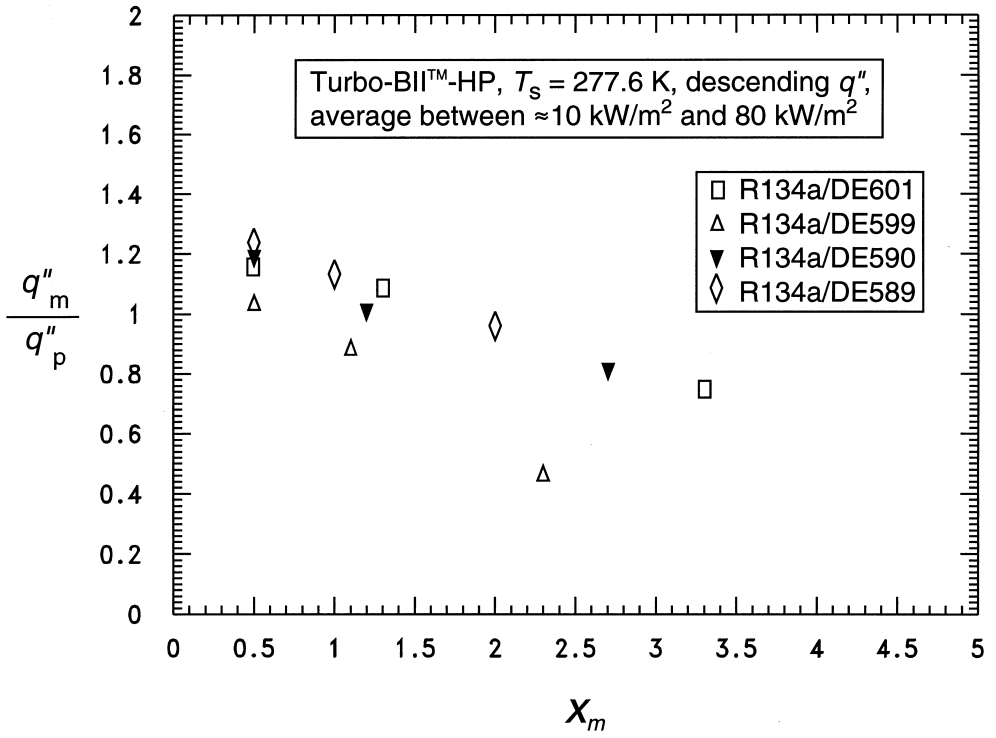

Fig. 11. Influence of lubricant mass fraction on R134a/lubricant pool boiling.

Fig. 11. Influence de la fraction massique du lubrifiant sur l'ébullition libre du mélange R134a/lubrifiant.

(Γ) and/or increases in the bulk lubricant concentration (c):

$$d\sigma = -RT_e\Gamma d\ln c \tag{6}$$

where R is the universal gas constant, and T_e is the temperature of the interface. A heat transfer enhancement existed when the increase in site density more than compensates for the reduction in bubble size. However, as the lubricant mass fraction increases, the bubble size decreases while the site density increases. The Mikic and Rohsenow [31] pool boiling model shows that the heat flux is directly proportional to the product of the site density and the square of the bubble departure diameter. Consequently, the influence of the bubble size on the heat transfer is greater than that of the site density. As a result, the pool boiling heat transfer eventually degrades with increased lubricant mass fraction.

Even for small bulk lubricant mass fractions, a large lubricant viscosity benefits pool boiling by promoting a thick thermal boundary layer. The existence of the excess layer accentuates the influence of the lubricant properties on the heat transfer because pool boiling is controlled in large part by the fluid properties at the heated wall. Because of the excess layer, the viscosity of the liquid near the wall can be significantly greater than what it would have been for the bulk mixture. An estimate of the relative pool boiling thermal boundary layer thickness for two lubricants (subscripts 1 and 2) was derived from the model of Bosnjakovic [32] while assuming that the bubble frequency was not influenced by lubricant properties:

$$\frac{\delta_1}{\delta_2} = \sqrt{\frac{\nu_1 Pr_2}{\nu_2 Pr_1}} \tag{7}$$

In general, the Prandtl number (Pr) does not differ much from lubricant to lubricant despite a large variation in viscosity. Consequently, Eq. (7) shows that the thermal boundary layer is a strong function of viscosity providing a thicker thermal boundary layer for larger viscosities. A thicker thermal boundary, in turn, provides for a larger active site density [33], which improves the pool boiling heat transfer.

The lubricant excess layer and a thicker thermal boundary layer may reduce heat transfer by convection, but this is only a small component of the total boiling heat transfer. Boiling is sustained mainly from the energy that is stored in the thermal boundary layer. Consequently, the additional superheat that the bubble receives from the thicker thermal boundary layer more

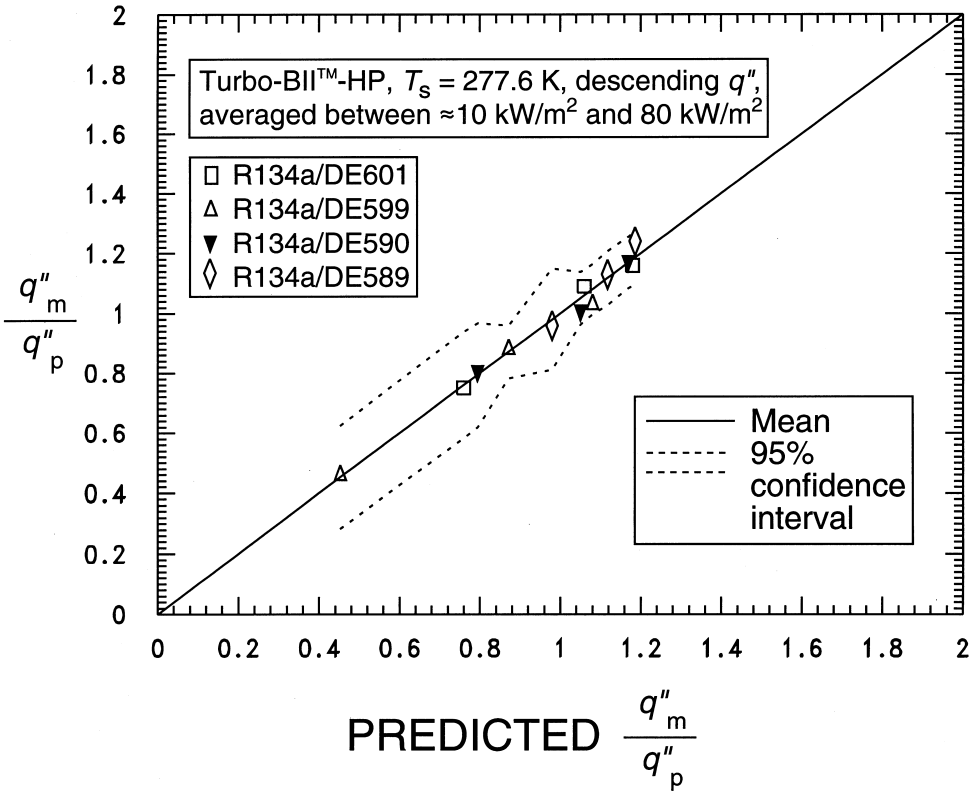

Fig. 12. Comparison of measured heat flux ratio to that predicted by Eq. (5).

Fig. 12. Comparaison du flux thermique mesuré et celui prévu par l'Equation 5.

than compensates for the reduced convection heat transfer.

The fact that viscosity and CST are coupled is analogous with the prediction of viscosity relative to the proximity of the CST. Laesecke [34] has observed that the deviation of the measured viscosity from an ideal mixing rule for R32/propane increases as the CST is approached. Laesecke [34] believes that the interaction between the polar R32 and the nonpolar propane is responsible for the nonideal behavior of the viscosity near the CST. Because the R134a/lubricant mixture is a polar/nonpolar mixture, a similar nonideal behavior of the viscosity near the CST should be expected. Although this does not explain the interdependence of the lubricant viscosity and the CST, it does establish precedence for the interaction that is quantified in Eq. (5).

The proximity of the bulk fluid temperature to the CST of the mixture benefits pool boiling heat transfer by the formation of additional excess liquid films that draw superheated liquid onto the bubble sides. Mitrovic [12] describes how a lubricant-rich film exists around the liquid-vapor interface of the refrigerant bubble. According to Jensen and Jackman [11], the lubricant-rich layer is formed by preferential evaporation of the refrigerant at the bubble's liquid–vapor interface. However, it is possible that the bubble may also lift a portion of the lubricant excess layer from the heated wall. In any case, given that an excess lubricant layer surrounds the bubble, Fig. 13 shows how a small difference between the bulk fluid temperature and the CST can dramatically affect the pool boiling heat transfer.

Fig. 13 shows a theoretical critical solution diagram for a refrigerant/lubricant mixture and a bubble on a heated wall. The critical solution diagram gives the temperature and the compositions for which the lubricant and refrigerant are miscible. Above the dome, the lubricant and refrigerant are completely miscible for all compositions. Within the dome, two soluble solutions of refrigerant and lubricant exist at different compositions. The closed circle on the critical solution diagram represents the state of the bulk liquid mixture that is close to, but greater than, the CST. The arrow shows how the state of the liquid in the immediate vicinity of the bubble transitions to a two-phase state by a combination of composition shifting and evaporation at the liquid–vapor interface. Once this happens, two thin layers of

different refrigerant/lubricant soluble solutions rest on the liquid–vapor interface of the bubble. Of course, only a partial separation is likely because of the short time available before the bubble temperature equilibrates with the bulk liquid. It is also likely that these films are actually liquid droplets that cover regions of the bubble but act like films due to the relative size of the bubble and the droplet. Droplets could also lie adjacent to rather than on top of one another. In any case, the interfaces of the two liquid films are drawn in Fig. 13 to have large curvature gradients. The curvature gradients induce film pressure gradients that transport superheated liquid to the sides of the bubble. The additional bubble superheat is the cause of the pool boiling heat transfer enhancement.

Another plausible mechanistic reason for the boiling enhancement obtained with lubricants that are partially miscible in the refrigerant is that liquid–liquid phase separation causes additional active sites. Oxtoby [35] shows that increased nucleation is possible for a mixture of water and hydrogen via liquid-like rather than vapor seed bubbles. Laesecke [34] suggests that because the volatility of the components of both the water/hydrogen mixture and the refrigerant/lubricant mixture differ greatly, the mixtures may exhibit similar phase separation behavior at the critical nucleus.

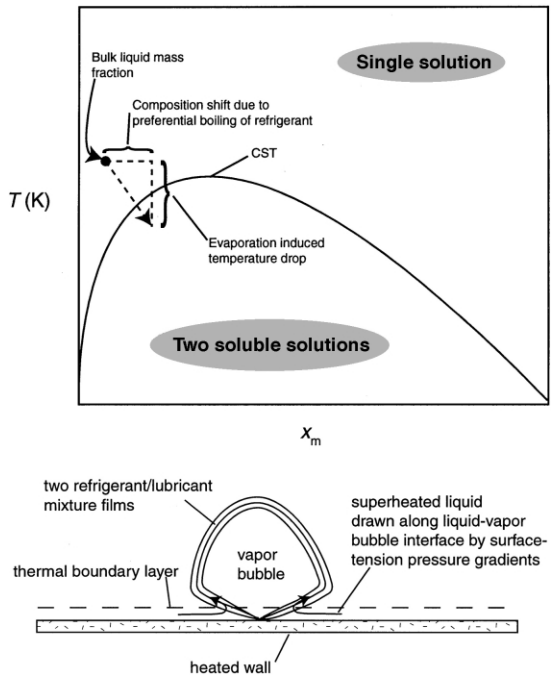

Fig. 13. Mechanistic explanation of the influence of lubricant miscibility on boiling.

Fig. 13. Fondement mécanique de l'influence de la miscibilité du lubrifiant sur l'ébullition.

8. Visual observations

The visual observations from the high-speed films showed that both the type of lubricant and the lubricant mass fraction had a marked effect on bubble formation. From past experience with visual observations, it was found that pure refrigerant bubbles reflected light readily; whereas, bubbles with lubricant appeared to be dull. In general, the refrigerant/lubricant combination that performed best was where the bubbles remained reflective for low and high lubricant concentrations. Heat transfer degradations with lubricants appeared to be associated with micro-size bubbles and/or a fog of bubbles. For example, the intermediate heat transfer R134a/DE590 mixture bubbles appeared clear or reflective at 0.5% mass fraction, and then they developed what appeared to be lubricant caps at 1% mass fraction. Then, finally, they developed into a fog of micro-bubbles at 2% lubricant mass fraction. Compare this to the high heat transfer bubbles for the R134a/DE590 mixture where lubricant caps did not appear on the bubbles until the 2% lubricant mass fraction. The low heat transfer bubbles of the R134a/DE599 mixture were misty for all lubricant mass fractions. In summary, R134a/lubricant mixtures that appeared to have less lubricant on the bubbles had superior pool boiling heat transfer performance.

9. Conclusions

The pool boiling heat transfer of 12 R134a/lubricant mixtures were compared to that of pure R134a on a Turbo-BII^{TM}-HP surface. The mixtures were chosen to examine the effects of lubricant mass fraction, viscosity, and miscibility on heat transfer performance. The range of the lubricant viscosity that was investigated was from 22 to 197 μm2/s. The critical solution temperature (CST) of the R134a lubricant mixtures ranged from 203 to 270 K. The lubricant mass fraction of the mixtures ranged from 0.5 to 3.3.

The magnitude of the effect of each parameter on the heat transfer data was quantified with a regression analysis. The mechanistic cause of each effect was given based on new theoretical interpretation and/or that from the literature. For example, the literature shows that the larger lubricant mass fractions promote smaller bubble departure diameters, which, in turn, leads to poorer heat transfer. New speculation suggests that the proximity of the bulk fluid temperature to the CST of the mixture benefits pool boiling heat transfer by the formation of additional excess liquid films that draw superheated liquid onto the bubble sides. In addition, even for small bulk lubricant mass fractions, a large lubricant viscosity benefits pool boiling by promoting a thick thermal boundary layer. To summarize, the model

illustrates that larger heat transfer enhancements can be obtained for small lubricant mass fraction, high lubricant viscosity, and a small difference between the refrigerant saturation temperature and the critical solution temperature of the lubricant.

The ratio of the heat flux of the R134a/lubricant mixture to that of the pure R134a for fixed wall superheat was given as a function of pure R134a heat flux for all twelve mixtures. The greatest heat flux ratio was obtained for the mixture with the lubricant that had the largest CST. For example, the pool boiling performance of R134a was enhanced as much as (100%±20%) by adding 0.5% mass lubricant DE589. Overall, the R134a/DE589 (99.5/0.5) mixture exhibited a 24% greater heat transfer than pure R134a from approximately 10 to 80 kW/m^2. The smallest heat flux ratio (0.45±0.09) was obtained for the mixture with the lubricant that had the smallest viscosity and the smallest CST with R134a.

Acknowledgements

This work was jointly funded by NIST, the US Department of Energy (project no. DE-01-91CE23808.000), and ICI. Mr. Esher Kweller and Mr. Bruce Gilbert were the Project Managers for DOE and ICI, respectively. All the lubricants of this study were specially fabricated for this project by ICI. Thanks go to the following ICI personnel for their helpful consultations: Dr. Stuart Corr, Dr. Thomas Dekleva, Dr. Thomas Murphy, and Mr. Robert Yost. Thanks also go to the following NIST personnel for their constructive criticism of the first draft of the manuscript: Dr. Piotr Domanski, Dr. Arno Laesecke, Mrs. Janet Land, and Dr. W. Vance Payne. The author would like to express appreciation to Mr. Edgar Bellinger and Mr. Joseph Crowder for data collection. Furthermore, the author extends appreciation to Dr. W. Guthury and Mr. A. Heckert for consulting on the uncertainty analysis. Special thanks goes to Mr. Petur Thors of Wolverine for donating the Turbo-BII^{TM}-HP surface. Thanks also go to Professor Arthur Bergles for his helpful suggestions.

References

[1] Sauer HJ, Gibson RK, Chongrungreong S. Influence of oil on the nucleate boiling of refrigerants, In: 6th Int. Heat Transfer Conf., vol. 1, Toronto, 1978. p. 181–6.

[2] Hahne E, Noworyta A. Calculation of heat transfer coefficients for nucleate boiling in binary mixtures of refrigerant–oil. Int Com Heat Mass Transfer 1984;11(5):417–27.

[3] Memory SB, Bertsch G, Marto PJ. Pool boiling of HCFC-124/oil mixtures from smooth and enhanced tubes (HTD-vol. 243), In: Heat transfer with alternative refrigerants, ASME, 1993. p. 9–18.

[4] Memory SB, Sugiyama DC, Marto PJ. Nucleate pool boiling of R-114 and R-114-oil mixtures from smooth and enhanced surfaces — I. Single tubes. Int J Heat Mass Transfer 1995;38(8):1347–61.

[5] Webb RL, McQuade WF. Pool boiling of R11 and R123 oil–refrigerant mixtures on plain and enhanced tube geometries. ASHRAE Trans 1993;99:1225–36.

[6] Bell KI, Hewitt GF, Morris SD. Nucleate pool boiling of refrigerant/oil mixtures. Experimental Heat Transfer 1987;1:71–86.

[7] Jabardo JMS, da Silva CL. Modeling of the nucleate boiling of refrigerant–oil mixtures. XVIIIth Int Congr of Refrigeration 1991;2:514–8.

[8] Rohsenow WM. A method of correlating heat transfer for surface boiling liquids. Transactions of ASME 1951;73: 969.

[9] Chongrungreong S, Sauer Jr HJ. Nucleate boiling performance of refrigerants and refrigerant–oil mixtures. J of Heat Transfer 1980;102:701–5.

[10] Stephan K. Influence of oil on heat transfer of boiling refrigerant 12 and refrigerant 22. In: XI Int. Congr. of Refrigeration, vol. 1. p. 369–380.

[11] Jensen MK, Jackman DL. Prediction of nucleate pool boiling heat transfer coefficients of refrigerant–oil mixtures. Journal of Heat Transfer 1984;106:184–90.

[12] Mitrovic J. Nucleate boiling of refrigerant-oil mixtures: bubble equilibrium and oil enrichment at the interface of a growing vapour bubble. Int J Heat Mass Transfer 1998; 41:3451–67.

[13] Burkhardt J, Hahne. Influence of oil on the nuncleate boiling of refrigerant 11. XVth Int Congr of Refrigeration 1979;2:537–43.

[14] Kedzierski MA. Simultaneous visual and calorimetric measurements of R11, R123, and R123/alkylbenzene nucleate flow boiling. In: Sauer Jr HJ, Tuehn TH, editors. Heat transfer with alternative refrigerants (ASME HTD-vol. 243). New York: ASME, 1992. p. 27–33.

[15] Kedzierski MA, Kaul MP. Horizontal nucleate flow boiling heat-transfer-coefficient measurements and visual observations for R12, R123, and R123/ester lubricant mixtures, In: 6th Int. Symp. on Transport Phenomena in Thermal Engineering, vol. 1, Seoul, Korea, p. 111–6.

[16] Kedzierski MA. Enhancement of R123 pool boiling by the addition of N-hexane. Journal of Enhanced Heat Transfer 1999;6(5):343–55.

[17] Kedzierski MA. Enhancement of R123 pool boiling by the addition of hydrocarbons. Int J Refrigeration 2000;23:89–100.

[18] Rosen MJ. Surfactants and interfacial phenomena. New York: John Wiley & Sons, 1978. p. 57

[19] Adamson AW. Physical chemistry of surfaces. 2nd ed. New York: Interscience Publ, 1967 p. 353.

[20] Bateman DJ. How necessary are oil changes with alternative refrigerants? Air Conditioning, Heating and Refrigeration News, 12 May 1997. p. 24.

[21] Didion DA. The application of HFCs as refrigerants. In: 20th Int. Congr. of Refrigeration, Keynote, 1999.

[22] Eckert ERG, Goldstein RJ. 1976. Measurements in heat transfer. 2nd Ed. Washington: Hemisphere. p. 9–11.

[23] Kedzierski MA, Worthington III JL. Design and machining of copper specimens with micro holes for accurate heat

transfer measurements. Experimental Heat Transfer 1993;6:329–44.
[24] Kedzierski MA. Calorimetric and visual measurements of R123 pool boiling on four enhanced surfaces (NISTIR 5732). Washington: US Department of Commerce, 1995.
[25] Kedzierski MA. The effect of lubricant concentration, miscibility, and viscosity on R134a pool boiling (NISTIR 6450). Washington: US Department of Commerce, 2000.
[26] Siu MCI, Carroll WL, Watson TW. Thermal conductivity and electrical resistivity of six copper-base alloys (NBSIR 76-1003). Washington: US Department of Commerce, 1976.
[27] Chen J, Tuzla K. Heat transfer characteristics of alternative refrigerants; vol. 3: condenser and evaporator outside tube. EPRI TR-106016-V3, project 3412-53, Palo Alto, 1996.
[28] Starner KE. Engineering consultant, private communications, York, PA, 2000.
[29] Cornwell K, Einarsson JG. The influence of fluid flow on nucleate boiling from a tube. In: Eurotherm Seminar No. 8, Advances in Pool Boiling Heat Transfer, Paderborn, FRG, 11–12 May 1989. p. 28–41.
[30] Sato T, Takaishi Y, Oguchi K. Concentration dependence of pool nucleate boiling heat transfer coefficients for R134a and pag oil system, In: 20th Int. Congr. of Refrigeration, IIR/IIF, Sydney, 1999.
[31] Mikic BB, Rohsenow WM. New correlations of pool boiling data including the effect of heating surface characteristics. J Heat Trans 1969;91:245–50.
[32] Bosnjakovic F. Verdampfung und fluessigheitsueberhitzung. Tech Mech Und Therm 1930;1:358–62.
[33] Hsu YY. On the size range of active nucleation cavities on a heating surface. J Heat Transfer 1962;84:207–16.
[34] Laesecke A. Private communications. NIST, Boulder, CO, 1999.
[35] Oxtoby DW. Nucleation of first-order phase transitions. Acc Chem Res 1998;31(2):91–7.
[36] Corr S. Private communications. ICI, Widnes, Cheshire, 1995.